

Abstract

The accuracy of ground deformation modelling at active volcanoes is a principal requirement in volcanic hazard mitigation. However, the reliability of such models relies on the accuracy of the rock physical property (permeability and elastic moduli) input parameters. Unfortunately, laboratory-derived values on representative rocks are usually rare. To this end we have performed a systematic laboratory study of the influence of pressure and temperature on the permeability and elastic moduli of the two most widespread tuffs from the Campi Flegrei volcanic district, Italy. Our data show that the water permeability of Neapolitan Yellow Tuff and a tuff from the Campanian Ignimbrite differ by about two orders of magnitude, highlighting the heterogeneous nature of the tuffs at Campi Flegrei. As pressure (depth) increases beyond the critical point for inelastic pore collapse (at an effective pressure of 10–15 MPa, or a depth of about 750 m), permeability and porosity decrease significantly, and ultrasonic wave velocities and dynamic elastic moduli increase significantly. Increasing the thermal stressing temperature increases the permeability and decreases the ultrasonic wave velocities and dynamic elastic moduli of the Neapolitan Yellow Tuff; whereas the tuff from the Campanian Ignimbrite remains unaffected. This difference is due the presence of thermally unstable zeolites within the Neapolitan Yellow Tuff. For both rocks we also find, under the same pressure conditions, that the dynamic (calculated from ultrasonic wave velocities) and static (calculated from triaxial stress-strain data) elastic moduli differ significantly. The choice of elastic moduli in ground deformation modelling is therefore an important consideration. While we urge that these new laboratory data should be considered in routine ground deformation modelling, we highlight the heterogeneous nature of the rocks that comprise the caldera at Campi Flegrei.

SED

5, 1081–1123, 2013

Permeability and elastic moduli of tuff

M. J. Heap et al.

Title Page

Abstract

Introduction

Conclusions

References

Tables

Figures

◀

▶

◀

▶

Back

Close

Full Screen / Esc

Printer-friendly Version

Interactive Discussion



1 Introduction

Monitoring ground deformation, the surface expression of deeper magmatic and/or hydrothermal activity, at active volcanoes is an important tool in volcanic hazard forecasting and mitigation. Ground deformation at a volcano (measured by global positioning system (GPS) satellites, interferometric synthetic aperture radar (InSAR), tiltmeters, or electronic distance metres, EDM) are typically analysed using inverse problem models that consider a source (e.g., a magma chamber, a zone of overpressurised fluids, or a combination of the two) embedded within a homogenous elastic or viscoelastic half-space (e.g., Mogi, 1958; Dzurisin, 2006; Hurwitz et al., 2007). These models yield important information regarding the location, shape, and volume/pressure changes of the source. The accuracy of such modelling relies on the accuracy of the rock physical property input parameters (typically elastic moduli and permeability, depending on the type of model). Even small changes in the values of key controlling parameters can lead to large differences in the rate, magnitude, and geometry of ground surface deformation (e.g., Hurwitz et al., 2007). For instance, a recent contribution using viscoelastic modelling to better understand flank motion and summit subsidence at Kīlauea (Hawai‘i) showed that deformation rates are enhanced when the elastic moduli input parameters are lowered (Plattner et al., 2013). Furthermore, homogenous half-space models, by definition, assume that the rocks that comprise the volcano have identical physical properties. However, volcanoes are built from successive eruptive episodes and thus the physical properties of the rock strata that form the edifice are likely to span a wide range. For this reason, conventional homogenous half-space modelling at volcanoes has recently been considered an oversimplification that could lead to misinterpretation of the derived source parameters (Manconi et al., 2007, 2010). For instance, Manconi et al. (2010) showed that this “standard” approach can lead to inaccurate values for the source volume changes. Therefore, models that consider mechanical heterogeneities (e.g., Manconi et al., 2007, 2010) require a good knowledge of the breadth of elastic moduli that can be expected for representative rocks, and hydrothermal fluid flow mod-

SED

5, 1081–1123, 2013

Permeability and elastic moduli of tuff

M. J. Heap et al.

Title Page

Abstract

Introduction

Conclusions

References

Tables

Figures

◀

▶

◀

▶

Back

Close

Full Screen / Esc

Printer-friendly Version

Interactive Discussion



els (e.g., Hurwitz et al., 2007; Todesco et al., 2010) require accurate values of their permeability and elastic moduli.

The densely populated (about 3 million) Neapolitan area, southern Italy, is in a state of constant threat provided by the proximity of the Campi Flegrei (CF) volcanic district, dominated by a 13 km wide resurgent, nested caldera that formed by a succession of collapse episodes following large phreatoplinian eruptions (e.g., Barberi et al., 1991; Orsi et al., 1992, 1996). The activity at CF can be characterised by two main eruptions: (1) the eruption related to the Campanian Ignimbrite about 37 000 yr ago and, (2) the eruption of the Neapolitan Yellow Tuff (NYT) about 12 000 yr ago (Di Vito et al., 1999). The caldera now hosts a large, shallow (< 4 km) hydrothermal system (e.g., De Natale et al., 2006). Although there has not been an eruption for almost half a century (since the Monte Nuovo eruption of 1538 AD), CF has become increasingly restless and is densely monitored by permanent seismic and ground deformation networks. Recently, two major episodes of unrest have occurred, between 1969–1972 and 1982–1984 (Bianchi et al., 1987; Bonafede, 1991). Surface uplift, on the order of several metres (bradyseism), and accompanying earthquakes in 1984 resulted in the evacuation of the town of Pozzuoli. Since then, there has been an overall subsidence trend, periodically interrupted by small (cm-scale) and short-lived (months) uplifts in 1989, 1994, 2000–2001 (Lanari et al., 2004; Bianco et al., 2004) and 2004–2006 (Saccorotti et al., 2007; Trasatti et al., 2008). The recent episodes of ground deformation and seismicity are considered to be the result of the interaction between the hydrothermal system and deeper magmatic gases; such interaction is a potential trigger for future unrest (e.g., Chiodini et al., 2003, 2010).

However, the interpretation of long-term and short-term ground deformation patterns at CF is heavily debated (e.g., Bonafede et al., 1986; Bianchi et al., 1987; Bonafede, 1991; De Natale et al., 1991, 2001, 2006; Gaeta et al., 1998; Bonafede and Mazzanti, 1998; Orsi et al., 1999; Lundgren et al., 2001; Troise et al., 2001; Gaeta et al., 2003; Beauducel et al., 2004; Lanari et al., 2004; Battaglia et al., 2006; Gottsmann et al., 2006; Bodnar et al., 2007; Trasatti et al., 2008; Manconi et al., 2010). Some models ex-

SED

5, 1081–1123, 2013

Permeability and elastic moduli of tuff

M. J. Heap et al.

Title Page

Abstract

Introduction

Conclusions

References

Tables

Figures

◀

▶

◀

▶

Back

Close

Full Screen / Esc

Printer-friendly Version

Interactive Discussion



Permeability and elastic moduli of tuff

M. J. Heap et al.

Title Page

Abstract

Introduction

Conclusions

References

Tables

Figures

I◀

▶I

◀

▶

Back

Close

Full Screen / Esc

Printer-friendly Version

Interactive Discussion



plain the measured surface deformation using a fluid-dynamical model (e.g., De Natale et al., 2001; Todesco et al., 2010), while others utilise boundary faults (e.g., Beauducel et al., 2004), vertical density stratification (Bonafede and Mazzanti, 1998), or mechanical heterogeneities (Manconi et al., 2010). As explained above, the accuracy of these models rely on accurate physical property input parameters of representative tuffs. Unfortunately, laboratory investigations on the physical properties of tuffs from CF are rare. Values of permeability have, thus far, either been inferred from in-situ observations (Rosi and Sbrana, 1987) or have been taken from experiments conducted on NYT under ambient pressure conditions (Ascolese et al., 1993a, b; Peluso and Arienzo, 2007). In the most recent study, Peluso and Arienzo (2007) measured the permeability of NYT to be between 2.0×10^{-15} and $6.3 \times 10^{-17} \text{ m}^2$ (the range of porosity was between 48 and 52 vol.%). However, not only are the tuffs of CF present at depth (which is likely to severely influence their permeability), but it is known that the permeability of different tuffs can be highly variable (a variety of tuffs should therefore be measured), depending on their degree of lithification (Vinciguerra et al., 2009). Elastic moduli are generally assumed, or extrapolated from seismic tomography studies (e.g., Chiarabba and Moretti, 2006; Vinciguerra et al., 2006). Typically, Poisson's ratio is taken as 0.3 and shear modulus as 5 GPa. However, dynamically-determined elastic moduli (i.e., those from ultrasonic wave velocities) may not represent the most appropriate values to use in volcano ground deformation modelling. Deformation caused by a volcanic source proceeds quasi-statically rather than dynamically and therefore static elastic moduli are likely to be the most appropriate input parameters (Heap et al., 2009; Manconi et al., 2010). It is well known that dynamic and static moduli differ as a result of their large difference in frequency (Simmons and Brace, 1965; Cheng and Johnston, 1981; Eissa and Kazi, 1989; Ciccotti and Mulargia, 2004; Ciccotti et al., 2004). Static elastic moduli for representative materials from CF are not yet available (see Manconi et al., 2010).

The pyroclastic deposits that comprise the caldera at CF are exposed to elevated temperatures, as evidenced by two-dimensional conductive/convective numerical modelling (Wohletz et al., 1999), seismic attenuation tomography (de Lorenzo et al., 2001),

Permeability and elastic moduli of tuff

M. J. Heap et al.

Title Page

Abstract

Introduction

Conclusions

References

Tables

Figures

I◀

▶I

◀

▶

Back

Close

Full Screen / Esc

Printer-friendly Version

Interactive Discussion



and infrared imaging (Chiodini et al., 2007). Surface geothermal gradients of about $150\text{--}200\text{ }^{\circ}\text{C km}^{-1}$ are estimated (for the first 1.5 km) and, at the edge of the hydrothermal system, a temperature of $420\text{ }^{\circ}\text{C}$ was measured at a depth of 3 km (AGIP borehole San Vito 1, de Lorenzo et al., 2001). It has been shown previously that thermal stresses can increase the permeability (e.g., Homand-Etienne and Troalen, 1984; Jones et al., 1997; David et al., 1999; Nara et al., 2011) and decrease the Young's modulus (e.g., Keshavarz et al., 2010) of rock. This is usually interpreted as the formation of new microcracks due to the build-up of internal thermal stresses. Volcanic rocks, which are persistently challenged by elevated temperatures due to their proximity to large permanent heat sources, and the fluctuations in temperature caused by the movement of magma, are therefore especially prone to thermal microcracking. Furthermore, many fine-grained pyroclastic deposits (e.g., tuffs) can be further jeopardised by thermal stresses due to the presence of thermally unstable zeolites (Heap et al., 2012). Since zeolitization promoted their lithification, the loss of zeolites can impose dramatic consequences on the physical properties of tuff. Recent data has shown that NYT becomes structurally unstable upon exposure to high ($100\text{--}750\text{ }^{\circ}\text{C}$) temperatures, resulting in a severe decrease in uniaxial compressive strength and indirect tensile strength (Heap et al., 2012). A recent contribution by Manconi et al. (2010) highlighted the need for the evaluation of the temperature-dependence of the material properties of the tuffs at CF.

For the reasons outlined above we report a systematic study of the influence of pressure and temperature on the physical properties (permeability, porosity, ultrasonic velocities, and elastic moduli) of two tuffs (one zeolitized) from CF. We first present the investigated materials and methods. We then present our experimental results before discussing our data in terms of modelling at CF.

2 Materials investigated

Our experiments were performed on samples of Neapolitan Yellow Tuff (NYT) and grey Campanian Ignimbrite (WGI), the products of the two major eruptions (12 000 yr ago and 37 000 yr ago, respectively) at CF caldera (e.g., see Orsi et al., 1996), located a few kilometres west of the city of Naples, Italy. Our sample materials were collected from open quarries within the Campanian area (the same blocks used in Heap et al., 2012).

NYT and WGI contain average connected porosities of 44 and 49 vol.%, respectively (measured using the triple weight water saturation technique, Guéguen and Palciauskas, 1994). Photographs and optical microscopy photomicrographs of the samples are provided in Fig. 1 and their ambient pressure, “as-collected” (i.e., “natural” samples that have undergone no heating or deformation) physical properties are listed in Table 1. NYT (Fig. 1a and b), a trachytic pyroclastic deposit characterized by both pyrogenic and authigenic phases (de Gennaro et al., 2000), contains phenocrysts of sanidine, plagioclase, clinopyroxene, biotite, and minor amounts of Ti-magnetite and apatite within a matrix of lapilli and glass shard ash. X-ray diffraction pattern analysis has indicated the presence of phillipsite, chabazite, and analcime (Heap et al., 2012). The mean content of these zeolites in NYT can exceed 50 wt.% (e.g., de Gennaro et al., 1990, 2000). WGI (Fig. 1c and d), feldspathized by authigenic mineralization processes, is made up of reversely-graded black scoriae embedded in an ashy matrix with subordinate lithics and crystals (Cappelletti et al., 2003). WGI contains hypidiomorphic phenocrysts of alkali-feldspars with minor amounts of clinopyroxene, as well as microlites of alkali-feldspar, Ti-magnetite and apatite, giving the matrix a trachytic appearance. The matrix comprises well-sorted glass shards with occasional accretionary ash clots and porous lapilli fragments (Heap et al., 2012).

SED

5, 1081–1123, 2013

Permeability and elastic moduli of tuff

M. J. Heap et al.

Title Page

Abstract

Introduction

Conclusions

References

Tables

Figures

◀

▶

◀

▶

Back

Close

Full Screen / Esc

Printer-friendly Version

Interactive Discussion



3 Experimental methods

The caldera at CF hosts a large, shallow (< 4 km) hydrothermal system (e.g., De Natale et al., 2006). Indeed, laboratory studies have demonstrated that water-saturated ultrasonic velocities on tuffs from CF are more representative of the in-situ values than “dry” (measurements conducted on oven dried samples at ambient laboratory humidity) ultrasonic velocities (Zamora et al., 1994; Vanorio et al., 2005; Vinciguerra et al., 2006). Since the tuffs of CF are present at depth, and are likely to contain a fluid phase, we consider experimental values on pressurised, water-saturated samples as the most representative. Our experimental program was twofold. (1) Hydrostatic (i.e., $\sigma_1 = \sigma_2 = \sigma_3$) experiments to measure changes in permeability, porosity, ultrasonic wave velocities, and dynamic elastic moduli with increasing effective pressure (P_{eff} , from 5 MPa to 50 MPa) on samples thermal stressed to a range of temperatures (from as-collected to 1000 °C). (2) Constant strain rate conventional triaxial (i.e., $\sigma_1 > \sigma_2 = \sigma_3$) deformation experiments at a P_{eff} of 5 MPa to measure static elastic moduli. Importantly, we measure both static and dynamic elastic moduli at the same P_{eff} (= 5 MPa) so that the values can be easily compared. All our experiments were performed at room temperature (while this may not accurately represent the natural case, we note that, to explore the influence of temperature on the physical properties of the tuffs, we conducted experiments on samples thermally stressed to a range of temperatures).

3.1 Hydrostatic experiments

Hydrostatic experiments were performed in the Rock and Ice Physics Laboratory (RIPL) at University College London (UCL) using a 300 MPa hydrostatic pressure vessel equipped with two 70 MPa servo-controlled pore fluid intensifiers or volumeters (Fig. 2, see also Kolzenburg et al., 2012). The apparatus is designed to measure permeability, porosity, and ultrasonic wave velocities contemporaneously. In our experiments we chose an experimental pressure range of 5–50 MPa (i.e., up to a depth of about 2.5 km). While we are aware that these pressures may exceed those expected

SED

5, 1081–1123, 2013

Permeability and elastic moduli of tuff

M. J. Heap et al.

Title Page

Abstract

Introduction

Conclusions

References

Tables

Figures

◀

▶

◀

▶

Back

Close

Full Screen / Esc

Printer-friendly Version

Interactive Discussion



for the tuffs within CF, we show an extended range simply to offer a more complete investigation of the physical properties of our materials.

Cylindrical samples, 25 mm in diameter and nominally 40 mm in length, were all cored from the same set of blocks and in the same orientation. Samples were precision ground so that their end faces were flat and parallel. Prior to experimentation, samples were either: (1) held at ambient temperature (as-collected) or, (2) thermally stressed to pre-determined temperatures of 100, 200, 300, 500, 750, or 1000 °C (note: NYT could not be tested after exposure to 1000 °C due to a severe volume reduction). Thermal stressing was achieved by heating the sample to the target temperature at a rate of 1 °C min⁻¹, holding the temperature constant for 60 min, and then cooling at the same rate. Once at room temperature, all samples were vacuum-saturated in distilled water prior to experimentation. The measured sample was then inserted into a nitrile rubber jacket and fixed between the two endcaps. The sample assembly was then lowered into the pressure vessel. Once inside the setup, the confining pressure (P_c) and the pore fluid (distilled water) pressure in both the “upstream” (P_{up}) and “downstream” (P_{down}) pore volumeters were increased to 10 and 5 MPa, respectively. The confining and pore pressures were increased slowly to avoid damaging the sample, and care was taken to ensure the sample was not pressurised beyond the maximum effective pressure targeted for the experiments (5 MPa). For the purpose of this study we apply the simple effective pressure law of $P_{eff} = P_c - \alpha P_p$, assuming that poroelastic constant $\alpha = 1$ (Guéguen and Palciauskas, 1994). The sample was left for 30 min at an effective pressure of 5 MPa to ensure microstructural equilibration and complete saturation.

Once equilibration at $P_{eff} = 5$ MPa was complete, the first ultrasonic measurements were taken. Ultrasonic waves velocities were measured via PZT piezoelectric P and S wave transducer crystals housed in the sample endcaps (Fig. 2) using an Agilent Technologies 1.5 GHz “Infiniium” digital storage oscilloscope and a JSR DPR300 35 MHz ultrasonic pulser/receiver. Dynamic elastic moduli were calculated from the resultant ultrasonic wave velocities using the following formulae (Guéguen and Palci-

SED

5, 1081–1123, 2013

Permeability and elastic moduli of tuff

M. J. Heap et al.

Title Page

Abstract

Introduction

Conclusions

References

Tables

Figures

◀

▶

◀

▶

Back

Close

Full Screen / Esc

Printer-friendly Version

Interactive Discussion



auskas, 1994):

$$E_d = \rho \frac{V_S^2 (3V_P^2 - 4V_S^2)}{V_P^2 - V_S^2} \quad (1)$$

$$v_d = \frac{V_P^2 - 2V_S^2}{2(V_P^2 - V_S^2)} \quad (2)$$

$$\mu_d = \frac{E_d}{2(1 + v_d)} \quad (3)$$

Where E_d is the Young's modulus, v_d is the Poisson's ratio, μ_d is the shear modulus, ρ is the bulk sample density and V_P and V_S are the P and S wave velocities, respectively.

Water permeability measurements were made by imposing a 1 MPa pressure difference across the jacketed sample. To achieve this, P_{up} and P_{down} were set at 4.5 and 5.5 MPa, respectively. The volumeters were then allowed to move full stroke (10 cm³) and steady-state flow was only assumed when the flow rate was constant over a protracted period. Water permeability (κ_{water}) was then calculated directly from Darcy's law:

$$\frac{Q}{A} = \frac{\kappa_{water}}{\eta L} (P_{up} - P_{down}) \quad (4)$$

where Q is the fluid volume flux, A is the cross-sectional area of the sample, η is the viscosity of the pore fluid, L is the length of the sample, and P_{up} and P_{down} are the pore pressures at the "upstream" and "downstream" ends of the sample, respectively.

Once the permeability measurement was complete, the "downstream" volumeter was isolated and the "upstream" volumeter was set back at 5 MPa. The P_c was then slowly increased to 15 MPa. By monitoring the movement of the "upstream" volumeter the porosity change from $P_{eff} = 5$ MPa to $P_{eff} = 10$ MPa could be accurately calcu-

SED

5, 1081–1123, 2013

Permeability and elastic moduli of tuff

M. J. Heap et al.

Title Page

Abstract

Introduction

Conclusions

References

Tables

Figures

◀

▶

◀

▶

Back

Close

Full Screen / Esc

Printer-friendly Version

Interactive Discussion



lated. The sample was then left for 30 min at the new pressure to ensure microstructural equilibration. Once equilibration was complete, the ultrasonic measurements for $P_{\text{eff}} = 10$ MPa were taken. This procedure was repeated for every 5 MPa P_{eff} increment up to 50 MPa.

5 During our experiments, the length of the sample L and the cross-sectional area A will change due to the compaction of the sample at elevated pressure. We have corrected for this (in our calculations of permeability and ultrasonic wave velocities) using the volume reduction of our sample (as measured by the water expelled from the sample) at each pressure interval, assuming isotropic compaction.

10 3.2 Triaxial deformation experiments

Constant strain rate ($1.0 \times 10^{-5} \text{ s}^{-1}$) conventional (i.e., $\sigma_1 > \sigma_2 = \sigma_3$) triaxial experiments were performed on as-collected cylindrical samples of the two tuffs (20 mm in diameter and nominally 40 mm in length). Samples were cored from the same blocks and in the same direction as for the permeability experiments. The samples were precision ground so that their end faces were flat and parallel. Experiments were all performed in the conventional triaxial deformation apparatus (Fig. 3) at the Laboratoire de Déformation des Roches (Université de Strasbourg) at a P_{eff} of 5 MPa (P_p of 5 MPa and a P_c of 10 MPa). Axial stress and strain were monitored continuously using a load cell and an LVDT displacement transducer, respectively. Pore volume change (used as a proxy for volumetric strain, ε_v) was monitored using a pore pressure intensifier, and the output of acoustic emissions (AEs) by a piezoelectric transducer crystal (located on the top of the piston) using a Physical Acoustics USB AE Node. AEs are high frequency elastic wave packets generated by the rapid release of strain energy such as during brittle microfracturing (see Lockner, 1993 for a review). During experimentation, an AE hit was recorded if a signal exceeded the set threshold of 40 dB. The AE “energy” (the area under the received AE waveform envelope) of each received AE signal was provided by the AEwin software. In this study we will adopt the convention that compressive stresses and compactive strains are positive.

Title Page

Abstract

Introduction

Conclusions

References

Tables

Figures

◀

▶

◀

▶

Back

Close

Full Screen / Esc

Printer-friendly Version

Interactive Discussion



Static Young's moduli (E_s) and Poisson's ratio (ν_s) were then calculated from the resultant stress-strain data, following the method of Heap and Faulkner (2008). We take both from the quasi-linear elastic regions of our tangent modulus curves (i.e., those regions where the moduli did not change). Static Poisson's ratio is given by:

$$5 \quad \nu_s = -\frac{\varepsilon_r}{\varepsilon_a} \quad (5)$$

where

$$\varepsilon_r = \frac{\varepsilon_v - \varepsilon_a}{2} \quad (6)$$

Where ε_r and ε_a are the radial and axial strain, respectively. Static shear modulus (μ_s) was then calculated using the following formula (Guéguen and Palciauskas, 1994):

$$10 \quad \mu_s = \frac{E_s}{2(1 + \nu_s)} \quad (7)$$

4 Results

4.1 The evolution of porosity with increasing pressure and temperature

The evolution of porosity with increasing P_{eff} (commonly called “hydrostats”) for NYT and WGI at each thermal stressing temperature is displayed in Fig. 4. For porous rock, an increase in hydrostatic pressure results in a volume and porosity decrease. Initially, this compaction is elastic (i.e., recoverable) but, at a critical pressure (assuming the rock is porous enough), pore collapse and grain crushing (now non-recoverable damage) ensues and the rate of compaction accelerates. This critical pressure is denoted P^* (Wong and Baud, 2012). The P_{eff} required to reach P^* varies from rock to rock, but largely depends on the initial rock porosity and grain size (generally, the higher the porosity, the lower the P_{eff} for P^*). The stress at which P^* occurs can therefore provide

Title Page

Abstract

Introduction

Conclusions

References

Tables

Figures

◀

▶

◀

▶

Back

Close

Full Screen / Esc

Printer-friendly Version

Interactive Discussion



Permeability and elastic moduli of tuff

M. J. Heap et al.

Title Page

Abstract

Introduction

Conclusions

References

Tables

Figures

◀

▶

◀

▶

Back

Close

Full Screen / Esc

Printer-friendly Version

Interactive Discussion



important information on the physical and microstructural state of rock at depth. In our experiments, the position of P^* is about 10 MPa for NYT and about 10–15 MPa for WGI (Fig. 4). Prior to P^* , during elastic compaction, we note that the porosity change is linear (i.e., there is no concave portion that is usually attributed to the closure of microcracks; however we note that this may be a result of the large steps in P_{eff} between measurements). Indeed, there is no microstructural evidence for microcracks in the as-collected materials (see Fig. 1). Immediately following P^* , during inelastic compaction, there is a dramatic increase in the rate of porosity reduction, as inelastic compaction proceeds. However, the porosity reduction rate then gradually decreases (especially above about 20 MPa). This represents the hardening of the rock due to compaction. Over the entire pressure range (up to 50 MPa) the porosity change for the as-collected sample is about the same for NYT and WGI (between 9 and 10 vol.%). Figure 4 also shows that the porosity evolution for WGI with increasing P_{eff} is unaffected by thermal stressing. By contrast, in the case of NYT, the porosity change decreases significantly as thermal stressing temperature increases. It can also be seen that, for both tuffs, thermal stressing does not appear to influence the position of P^* .

4.2 The evolution of permeability with increasing pressure and temperature

The evolution of permeability with increasing P_{eff} for NYT and WGI at each thermal stressing temperature is displayed in Fig. 5 (the values are reported in Tables 2 and 3). Firstly, we notice that the as-collected permeability of the two samples is very different. For instance, at a P_{eff} of 5 MPa, the permeability is about 1.0×10^{-15} and $1.0 \times 10^{-13} \text{ m}^2$ for NYT and WGI, respectively.

For WGI, the permeability curves show little change between 5 and 15 MPa. However, above 15 MPa, the permeability starts to decrease rapidly before reaching an apparent plateau above about 30 MPa. We note that this rapid decrease starts at the same pressure as the onset of inelastic compaction (P^*). Overall, the permeability is reduced by about an order of magnitude from $1.0 \times 10^{-13} \text{ m}^2$ at 5 MPa to $1.0 \times 10^{-14} \text{ m}^2$ at 50 MPa. The permeability curves for WGI show no clear trend with increasing thermal

stressing temperature. The different values obtained for the different thermal stressing temperatures are well within the expected range of natural variability between different samples cored from the same block.

However, there is a clear influence of the thermal stressing temperature on the permeability of NYT. At a P_{eff} of 5 MPa, the permeability increases from $1.0 \times 10^{-15} \text{ m}^2$ for the as-collected sample to $1.1 \times 10^{-14} \text{ m}^2$ for the sample thermally stressed to 750°C , an increase of an order of magnitude. As for the WGI, the permeability curves show little change between 5 and 10 MPa, after which permeability decreases more rapidly. We again note that this rapid decrease starts at the same pressure as the onset of inelastic compaction (P^*). Over the entire pressure range, the permeability is reduced by about an order of magnitude for the as-collected sample and by about three orders of magnitude for the sample thermally stressed to 750°C . Further, the total decrease in permeability increases with increasing thermal stressing temperature. The permeability curves all converge at about 40 MPa (at a permeability of about $4.0 \times 10^{-17} \text{ m}^2$). Therefore, at P_{eff} s of 40 MPa and above, there is no longer any influence of thermal stressing on the permeability of NYT.

4.3 The evolution of ultrasonic velocities and dynamic elastic moduli with increasing pressure and temperature

The evolution of the tuff physical properties (ultrasonic wave velocities, dynamic elastic moduli, and V_P/V_S ratio) for NYT and WGI are shown in Figs. 6 and 7, respectively. Firstly, it can be remarked that the as-collected physical properties of the two tuffs are similar (see also Table 1). For both tuffs, P and S wave velocity, dynamic Young's modulus, dynamic Poisson's ratio, and V_P/V_S ratio all increase with increasing P_{eff} , and in a similar manner. For example, for the as-collected NYT sample, P wave velocity increases by 40 %, S wave velocity by 21 %, Young's modulus by 53 %, Poisson's ratio by 19 %, shear modulus by 47 %, and V_P/V_S ratio by 15 % over the entire pressure range (5 to 50 MPa). The relative increases are similar for both tuffs. However, whereas the results for NYT (Fig. 6) show a systematic decrease in all the physical properties with

Permeability and elastic moduli of tuff

M. J. Heap et al.

Title Page

Abstract

Introduction

Conclusions

References

Tables

Figures

◀

▶

◀

▶

Back

Close

Full Screen / Esc

Printer-friendly Version

Interactive Discussion



increasing thermal stressing temperature, no systematic pattern can be discerned in the WGI results (Fig. 7). At a constant P_{eff} , thermal stressing decreases P and S wave velocity, dynamic Young's modulus, dynamic Poisson's ratio, and V_P/V_S ratio in NYT. For example, for NYT at a P_{eff} of 5 MPa, P wave velocity decreases by 21 %, S wave velocity by 4 %, Young's modulus by 18 %, Poisson's ratio by 56 %, shear modulus by 8 %, and V_P/V_S ratio by 17 % over the entire temperature range (as-collected to 750 °C).

4.4 Static elastic moduli under triaxial conditions

The differential stress-axial strain curves and associated AE energy output curves for the triaxial experiments are shown in Fig. 8, and the differential stress-porosity reduction curves are shown in Fig. 9. Even at a P_{eff} as low as 5 MPa, the deformation behaviour of the two tuffs can be described as macroscopically ductile (i.e., their ability to resist load did not decrease, see Rutter, 1986). For both rocks, a critical pressure, termed C^* (Wong and Baud, 2012), is reached which marks the point where there is an acceleration in axial strain (Fig. 8) and porosity reduction (or volumetric strain, Fig. 9) for a given stress increment. This phenomenon is called "shear-enhanced compaction", and beyond C^* the rocks are deforming in the compactive cataclastic flow regime which, in this case, is associated with strain hardening. In our experiments, C^* occurs at differential stresses of about 4.5 and 9 MPa for NYT and WGI, respectively. This contrasts with the values for P^* of 10 and 15 MPa, respectively, and demonstrates how the application of shear stresses enhances compactive deformation. Although this mode of failure differs greatly from the brittle failure seen in the uniaxial experiments of Heap et al. (2012) on the same rocks, both deformation mechanisms involve the same micromechanical process: microcracking (as evidenced by the output of AE energy). However, whereas strain localisation is seen in the brittle field, cataclastic flow involves distributed microcracking (i.e., localisation did not occur). Indeed, we see no evidence for strain localisation in the post-experimental samples. The output of AE energy is seen to increase in a somewhat stepwise manner for both rocks (Fig. 8), reflecting bursts of microcracking events during deformation, we note that the average rate of AE

Title Page

Abstract

Introduction

Conclusions

References

Tables

Figures

◀

▶

◀

▶

Back

Close

Full Screen / Esc

Printer-friendly Version

Interactive Discussion



energy output for WGI is some 20 times higher than for NYT. The difference in AE energy output during deformation is likely to be the result of the compositional differences between the two tuffs.

Values for the static Young's modulus, static Poisson's ratio, and static shear modulus were calculated from the elastic portions of the stress-strain curves and are given in Table 4, together with dynamic values determined at the same pressure ($P_{\text{eff}} = 5 \text{ MPa}$) for comparison. We note that both the static Young's modulus and the static shear modulus are significantly lower than the corresponding dynamic values.

5 Discussion

5.1 Fluid flow and physical property evolution with depth

Our experimental data show that the water permeabilities of different as-collected tuff samples from Campi Flegrei can vary by multiple orders of magnitude (at a P_{eff} of 5 MPa, permeabilities are 1.0×10^{-15} and 1.0×10^{-13} for NYT and WGI, respectively). This permeability range could be considered surprising due to their similar porosities (44 and 49 vol.% for NYT and WGI, respectively). The difference is likely related to the extent of zeolitization and lithification; a similar conclusion to that drawn by Vinciguerra et al. (2009). Vinciguerra et al. (2009) measured the permeability of two different tuffs from the Alban Hills (Italy) and found that, at a P_{eff} of 5 MPa, the permeabilities of the two tuffs were significantly different. While the first (well-lithified, zeolitized facies with an average porosity of 14 vol.%) was found to have a permeability of about 10^{-18} m^2 , which decreased by about an order of magnitude upon the application of a P_{eff} of 70 MPa, the second (fine-grained, matrix-supported facies with frequent cm-sized accretionary lapilli and an average porosity of 18 vol.%) had a much higher permeability (about 10^{-15} m^2) that decreased by about two orders of magnitude over the same pressure range. Further, considering the high porosities of NYT and WGI, their permeabilities are actually surprisingly low; considered to be a consequence of their

SED

5, 1081–1123, 2013

Permeability and elastic moduli of tuff

M. J. Heap et al.

Title Page

Abstract

Introduction

Conclusions

References

Tables

Figures

◀

▶

◀

▶

Back

Close

Full Screen / Esc

Printer-friendly Version

Interactive Discussion



complex pore structure. By contrast, Boise sandstone (porosity of 35 vol.%), a rock with a much simpler microstructure, has a permeability of $1.8 \times 10^{-12} \text{ m}^2$ at a P_{eff} of 5 MPa (Zhu and Wong, 1997).

Our experimental data also show that the permeability of the two tuffs is reduced by about an order of magnitude over the pressure range from 5 MPa to 50 MPa. In detail, the reduction in permeability with increasing P_{eff} is very modest up to a P_{eff} of about 10–15 MPa, and accelerates at pressures above 10–15 MPa. This can be explained by the position of P^* (Fig. 4), the onset of inelastic pore collapse and grain crushing. As pores collapse and grains crushed, the effective pathways for fluid flow are reduced. This inelastic compaction also has a significant influence on other physical properties of the tuffs (ultrasonic wave velocities, dynamic elastic moduli, and the V_P/V_S ratio all increase), in agreement with similar studies on NYT (Vanorio et al., 2002; Vinciguerra et al., 2006). Evidence of pore collapse is illustrated in the scanning electron microscope image of a sample of NYT taken beyond P^* provided as Fig. 10. Pore collapse above P^* has previously been observed in a tuff from the Alban Hills, Italy (Zhu et al., 2011). A pressure of about 10–15 MPa roughly equates to a depth of about 750 m. Geological cross sections of CF (e.g., Orsi et al., 1996) suggest therefore that a large volume of the NYT and WGI tuffs are located at depths where the pressure will be above P^* .

5.2 The influence of temperature on fluid flow and physical properties

Our experimental data show that thermal stressing has a strong influence on the physical properties of NYT, whereas those for WGI are relatively unaffected. The fluid flow properties of NYT are enhanced (especially at shallow depths) upon exposure to high temperatures, and the ultrasonic wave velocities, dynamic elastic moduli, and the V_P/V_S ratio decrease. Thermal stressing has previously shown to decrease ultrasonic wave velocities in tuff from CF (Vinciguerra et al., 2006). The marked difference in the temperature-dependence of the physical properties between the two tuffs is likely due to the presence of significant quantities of thermally unstable zeolites in NYT, namely

Permeability and elastic moduli of tuff

M. J. Heap et al.

Title Page

Abstract

Introduction

Conclusions

References

Tables

Figures

◀

▶

◀

▶

Back

Close

Full Screen / Esc

Printer-friendly Version

Interactive Discussion



Permeability and elastic moduli of tuff

M. J. Heap et al.

Title Page

Abstract

Introduction

Conclusions

References

Tables

Figures

◀

▶

◀

▶

Back

Close

Full Screen / Esc

Printer-friendly Version

Interactive Discussion



phillipsite and chabazite, that are not present in WGI. Previous work combining thermo-gravimetric analysis, optical microscopy, and X-ray diffraction has indicated that, at 1000 °C, NYT lost 18 % of its initial mass, contained large numbers of macrocracks, and no longer contained any zeolites. Optical microscope photomicrographs of NYT thermally stressed to a temperature of 1000 °C are provided as Fig. 11. By contrast, no changes were seen in WGI heated to the same temperature (Heap et al., 2012). Since, phillipsite and chabazite represent the “cement” that promoted the lithification of the originally incoherent pozzolanic material constituting NYT (de Gennaro et al., 2000), the structural integrity of NYT deteriorates significantly upon their loss (Heap et al., 2012). Detailed studies on the thermal decomposition of the zeolites in NYT have highlighted that analcime loses water irreversibly, and that chabazite and phillipsite undergo a partial reversible dehydration at 240 °C. Phillipsite breaks down during dehydration and chabazite undergoes reversible hydration at 350 °C, and, by 900 °C, the structure of the zeolites will be so damaged that no further water molecules can be stored (de Gennaro and Colella, 1989). Therefore, the reported changes in NYT physical properties are due to a combination of thermal cracking and the disintegration of the material through the loss of zeolites.

If we consider NYT at a depth of 1 km, the geothermal gradients provided by the AGIP (1987) exploration boreholes show that temperatures of 200–250 °C are not unreasonable (Wohletz et al., 1999; de Lorenzo et al., 2001). The data of this study reveal that the zeolitized NYT are prone to undesirable thermal alteration at these temperatures. At temperatures of 200–250 °C, permeability increases by a factor of 2.5, ultrasonic wave velocities, dynamic elastic moduli, and V_P/V_S ratio decrease by roughly 10 %; and uniaxial compressive strength and indirect tensile strength are reduced by more than a factor of 2 (Heap et al., 2012). A reduction in tensile strength may further promote physical property changes by encouraging fluid pressure driven fracturing. An internal pore fluid pressure of 22–23 MPa (under a confining pressure of 6–7 MPa) was enough to fracture a sandstone of 13 vol.% porosity (Vinciguerra et al., 2004). It is therefore likely that the estimated overpressures needed to explain the ground defor-

mation at CF (e.g., 10 MPa, Gaeta et al., 1998) are sufficient to fracture the tuffs and cause further changes in rock physical properties.

5.3 Application of these data to ground deformation modelling at CF

Our data highlights that the elastic moduli of two different tuffs from CF can be quantitatively similar. Although this result supports the notion of a homogenous half-space model, we note that the elastic moduli are significantly depth-dependent (Figs. 6 and 7). Further, due the extreme variability of the tuffs within the caldera, we anticipate that definitive conclusions cannot be drawn without a systematic approach involving borehole samples from different depths and locations within the caldera (discussed further at the end of the section). However, and perhaps more pertinent for ground deformation modelling, we find that static and dynamic moduli for the same tuff differ substantially. Although it is not uncommon for static and dynamic elastic moduli to be different, due to their frequency-dependence (Simmons and Brace, 1965; Cheng and Johnston, 1981; Eissa and Kazi, 1989; Ciccotti and Mulargia, 2004; Ciccotti et al., 2004), it raises an important question regarding which values are more appropriate in modelling. Manconi et al. (2010) highlighted that, while dynamic elastic constants (those derived from seismic velocities) are representative for rock subject to a dynamic stress, perhaps static values are more appropriate in the analysis of deformation caused by volcanic sources. A similar conclusion was drawn by Heap et al. (2009). However, static elastic moduli for representative rocks at CF have not been available until now. Thus far, elastic moduli have been generally assumed, or extrapolated from seismic tomography studies (e.g., Chiarabba and Moretti, 2006). Typically, Poisson's ratio is taken as 0.3 and shear modulus as 5 GPa (e.g., De Natale et al., 1991). However, while our data shows that static and dynamic Poisson's ratio is similar for the measured tuffs (and equal to about 0.3), we also observe that the static shear modulus is about a factor of four lower than the dynamic value (Table 4). If one were to assume that our static values are representative, then a more suitable shear modulus would be 0.5 GPa, an order of magnitude lower than the values typically used in ground deformation modelling at CF.

Permeability and elastic moduli of tuff

M. J. Heap et al.

Title Page

Abstract

Introduction

Conclusions

References

Tables

Figures

◀

▶

◀

▶

Back

Close

Full Screen / Esc

Printer-friendly Version

Interactive Discussion



collected from an open quarry and may therefore not represent the material at depth (which have had time to compact, lithify, undergo chemical alteration . . .). Indeed, an unpublished pilot study by Sammonds et al. (2008) shows that some of the samples taken from the AGIP boreholes have undergone considerable compaction. Further, the tuffs of CF are likely to be extremely variable vertically and laterally (due to variable lithification, zeolitization, interaction with fluids and temperatures . . .), even within the same lithological unit, and therefore their physical properties are likely to span a wide range. It is clear that systematic measurements on deep scientific borehole samples are now needed from multiple locations and depths within the caldera.

6 Conclusions

1. Our experimental data show that the permeabilities of tuffs from Campi Flegrei (the Neapolitan Yellow Tuff and a tuff from the Campanian Ignimbrite) can vary by multiple orders of magnitude. Despite this, our data also show that their elastic moduli are similar; however, we note that dynamic and static moduli differ greatly. These data emphasize the heterogeneous nature of the tuffs that comprise the caldera at Campi Flegrei.
2. Increasing the effective pressure from 5 MPa to 50 MPa results in a permeability reduction of about an order of magnitude and a porosity reduction between 5 and 10 vol.% for both tuffs. As effective pressure increases we also observe an increase in ultrasonic wave velocities, dynamic elastic moduli, and V_P/V_S ratio. These changes all accelerate after the onset inelastic pore collapse (P^*), which exists between effective pressures of 10–15 MPa.
3. Thermal stressing increases the permeability and decreases the ultrasonic wave velocities, dynamic elastic moduli, and V_P/V_S ratio of the Neapolitan Yellow Tuff. However, the tuff from the Campanian Ignimbrite is unaffected by thermal stressing. This is the result of the loss of thermally unstable zeolites, namely phillipsite

SED

5, 1081–1123, 2013

Permeability and elastic moduli of tuff

M. J. Heap et al.

Title Page

Abstract

Introduction

Conclusions

References

Tables

Figures

◀

▶

◀

▶

Back

Close

Full Screen / Esc

Printer-friendly Version

Interactive Discussion



and chabazite, in Neapolitan Yellow Tuff. For example, for the sample thermally stressed to 750 °C, the permeability at an effective pressure of 5 MPa increases by an order of magnitude relative to the as-collected material.

4. While we urge that these new laboratory data should be considered in routine ground deformation modelling, we highlight the heterogeneous nature of the rocks that comprise the caldera at Campi Flegrei.

Acknowledgements. We gratefully acknowledge John Bowles, Steve Boon and Neil Hughes (all UCL) for help and support during experimentation. We thank G. Orsi for the provision of the experimental materials, and Y. Lavallée for discussions. M. J. Heap acknowledges CNRS INSU grant “*Étude de la stabilité des édifices volcaniques*”. P. Baud and P. G. Meredith acknowledge the support of a CNRS PICS grant.

References

- AGIP: Geologia e Geofisica Del Sistema Geotermico Dei Campi Flegrei, Servizi Centrali per l'Esplorazione, SERG-MMESG, San Donato, 1987.
- Ascolese, E., Aurisicchio, A., Briggs-Smith, M., Mita, D. G., Perna, G., Rossi, S., and Gaeta, F. S.: Thermodynamics of water-permeated unwelded pyroclasts, 1: equilibrium properties, *J. Volcanol. Geoth. Res.*, 57, 219–233, 1993a.
- Ascolese, E., Aurisicchio, A., Briggs-Smith, M., Mita, D. G., Perna, G., Rossi, S., and Gaeta, F. S.: Thermodynamics of water-permeated unwelded pyroclasts, 2: non-equilibrium properties, *J. Volcanol. Geoth. Res.*, 59, 235–251, 1993b.
- Barberi, E., Cassano, E., La Torre, P., and Sbrana, A.: Structural evolution of Campi Flegrei caldera in light of volcanological and geophysical data, *J. Volcanol. Geoth. Res.*, 48, 33–49, 1991.
- Battaglia, M., Troise, C., Obrizzo, F., Pingue, F., and De Natale, G.: Evidence for fluid migration as the source of deformation at Campi Flegrei caldera (Italy), *Geophys. Res. Lett.*, 33, L01307, doi:10.1029/2005GL024904, 2006.
- Beauducel, F., De Natale, G., Obrizzo, F., and Pingue, F.: 3-D Modelling of Campi Flegrei ground deformations: role of caldera boundary discontinuities, *Pure Appl. Geophys.*, 161, 1329–1344, 2004.

SED

5, 1081–1123, 2013

Permeability and elastic moduli of tuff

M. J. Heap et al.

Title Page

Abstract

Introduction

Conclusions

References

Tables

Figures

◀

▶

◀

▶

Back

Close

Full Screen / Esc

Printer-friendly Version

Interactive Discussion



Permeability and elastic moduli of tuff

M. J. Heap et al.

Title Page

Abstract

Introduction

Conclusions

References

Tables

Figures

◀

▶

◀

▶

Back

Close

Full Screen / Esc

Printer-friendly Version

Interactive Discussion



Bianchi, R., Coradini, A., Federico, C., Giberti, G., Lanciano, P., Pozzi, J. P., Sartoris, G., and Scandone, R.: Modeling of surface deformation in volcanic areas: the 1970–1972 and 1982–1984 crises of Campi Flegrei, Italy, *J. Geophys. Res.*, 92, 14139–14150, 1987.

Bianco, F., Del Pezzo, E., Saccorotti, G., and Ventura, G.: The role of hydrothermal fluids in triggering the July–August 2000 seismic swarm at Campi Flegrei, Italy: evidence from seismological and mesostructural data, *J. Volcanol. Geoth. Res.*, 133, 229–246, 2004.

Bodnar, R. J., Cannatelli, C., De Vivo, B., Lima, A., Belkin, H. E., and Milia, A.: Quantitative model for magma degassing and ground deformation (bradyseism) at Campi Flegrei, Italy: implications for future eruptions, *Geology*, 35, 791–794, 2007.

Bonafede, M.: Hot fluid migration: an efficient source of ground deformation: application to the 1982–1985 crisis at Campi Flegrei – Italy, *J. Volcanol. Geoth. Res.*, 48, 187–198, 1991.

Bonafede, M. and Mazzanti, M.: Modelling gravity variations consistent with grounddeformation in the Campi Flegrei caldera (Italy), *J. Volcanol. Geoth. Res.*, 81, 137–157, 1998.

Bonafede, M., Dragoni, M., and Quarenì, F.: Displacement and stress fields produced by a centre of dilation and by a pressure source in a viscoelastic half space: application to the study of ground deformation and seismic activity at Campi Flegrei, Italy, *Geophys. J. Int.*, 87, 455–485, 1986.

Cappelletti, P., Cerri, G., Collettini, C., de Gennaro, M., Langella, A., Perrotta, A., and Scarpati, C.: Post-eruptive processes in the Campanian Ignimbrite, *Miner. Petrol.*, 79, 79–97, 2003.

Cheng, C. H. and Johnston, D. H.: Dynamic and static moduli, *Geophys. Res. Lett.*, 8, 39–42, 1981.

Chiarabba, C. and Moretti, M.: An insight into the unrest phenomena at the Campi Flegrei caldera from V_P and V_P/V_S tomography, *Terra Nova*, 18, 373–379, doi:10.1111/j.1365-3121.2006.00701.x, 2006.

Chiodini, G., Todesco, M., Caliro, S., Del Gaudio, C., Macedonio, G., and Russo, M.: Magma degassing as a trigger of bradyseismic events: the case of Phlegrean Fields (Italy), *Geophys. Res. Lett.*, 30, 1434, doi:10.1029/2002GL016790, 2003.

Chiodini, G., Vilardo, G., Augusti, V., Granieri, D., Caliro, S., Minopoli, C., and Terranova, C.: Thermal monitoring of hydrothermal activity by permanent infrared automatic stations: results obtained at Solfatara di Pozzuoli, Campi Flegrei (Italy), *J. Geophys. Res.*, 112, doi:10.1029/2007JB005140, 2007.

Permeability and elastic moduli of tuff

M. J. Heap et al.

Title Page

Abstract

Introduction

Conclusions

References

Tables

Figures

I◀

▶I

◀

▶

Back

Close

Full Screen / Esc

Printer-friendly Version

Interactive Discussion



Chiodini, G., Caliro, S., Cardellini, C., Granieri, D., Avino, R., Baldini, A., Donnini, M., Minopoli C.: Long-term variations of the Campi Flegrei, Italy, volcanic system as revealed by the monitoring of hydrothermal activity, *J. Geophys. Res.*, 115, B03205, doi:10.1029/2008JB006258, 2010.

5 Ciccotti, M. and Mulargia, F.: Differences between static and dynamic elastic moduli of a typical seismogenic rock, *Geophys. J. Int.*, 157, 474–477, 2004.

Ciccotti, M., Almagro, R., and Mulargia, F.: Static and dynamic moduli of the seismogenic layer in Italy, *Rock Mech. Rock Eng.*, 37, 229–238, doi:10.1007/s00603-003-0019-7, 2004.

10 David, C., Menéndez, B., and Darot, M.: Influence of stress-induced and thermal cracking on physical properties and microstructure of La Peyratte granite, *Int. J. Rock Mech. Min.*, 36, 433–448, 1999.

de Gennaro, M., Petrosino, S., Conte, M. T., Munno, R., and Colella, A.: Zeolite chemistry and distribution in a Neapolitan Yellow Tuff deposit, *Eur. J. Mineral.*, 2, 779–786, 1990.

15 de Gennaro, M., Cappelletti, P., Langella, A., Perrotta, A., and Scarpati, C.: Genesis of zeolites in the Neapolitan Yellow Tuff: geological, volcanological and mineralogical evidences, *Contrib. Mineral. Petr.*, 139, 17–35, 2000.

de Lorenzo, S., Gasparini, P., Mongelli, F., and Zollo, A.: Thermal state of the Campi Flegrei caldera inferred from seismic attenuation tomography, *J. Geodyn.*, 32, 467–486, 2001.

20 De Natale, G., Pingue, F., Allard, P., and Zollo, A.: Geophysical and geochemical modelling of the 1982–1984 unrest phenomena at Campi Flegrei calder (southern Italy), *J. Volcanol. Geoth. Res.*, 48, 199–222, 1991.

De Natale, G., Troise, C., and Pingue, F.: A mechanical fluid-dynamical model for ground movements at Campi Flegrei caldera, *J. Geodyn.*, 32, 487–517, 2001.

25 De Natale, G., Troise, C., Pingue, F., Mastrolorenzo, G., Pappalardo, L., Battaglia, M., and Boschi, E.: The Campi Flegrei caldera: unrest mechanisms and hazards, *Geol. Soc. Lond. Spec. Pub.*, 269, 25–45, 2006.

Di Vito, M., Isaia, R., Orsi, G., Southon, J., de Vita, S., D’Antonio, M., Pappalardo, L., and Piochi, M.: Volcanism and deformation since 12,000 years at the Campi Flegrei caldera (Italy), *J. Volcanol. Geoth. Res.*, 91, 221–246, 1999.

30 Dzurisin, D.: *Volcano Deformation*, Chichester, UK, Springer, ISBN:978-3540426424, 2006.

Eissa, E. A. and Kazi, A.: Relation between static and dynamic Young’s moduli of rocks, *Int. J. Rock Mech. Min.*, 25, 479–482, 1989.

SED

5, 1081–1123, 2013

Permeability and elastic moduli of tuff

M. J. Heap et al.

Title Page

Abstract

Introduction

Conclusions

References

Tables

Figures

◀

▶

◀

▶

Back

Close

Full Screen / Esc

Printer-friendly Version

Interactive Discussion



Gaeta, F. S., De Natale, G., Peluso, F., Mastrolorenzo, G., Castagnolo, D., Troise, C., Pingue, F., Mita, D. G., and Rossano, S.: Genesis and evolution of unrest episodes at Campi Flegrei caldera: the role of thermal fluid-dynamical processes in the geothermal system, *J. Geophys. Res.*, 103, 20921–20933, 1998.

5 Gaeta, F. S., Peluso, F., Arienzo, I., Castagnolo, D., De Natale, G., Milano, G., Albanese, C., and Mita, D. G.: A physical appraisal of a new aspect of bradyseism: the miniuplifts, *J. Geophys. Res.*, 108, B8, 2363, doi:10.1029/2002JB001913, 2003.

Gottsmann, J., Camacho, A. G., Tiampo, K. F., and Fernandez, J.: Spatiotemporal variations in vertical gravity gradients at the Campi Flegrei caldera (Italy): a case for source multiplicity during unrest?, *Geophys. J. Int.*, 167, 1089–1096, 2006.

10 Guéguen, Y. and Palciauskas, V.: *Introduction to the Physics of Rocks*, Princeton University Press, Princeton, New Jersey, 1994.

Heap, M. J. and Faulkner, D. R.: Quantifying the static elastic evolution of crystalline rock approaching failure, *Int. J. Rock Mech. Min.*, 45, 564–573, 2008.

15 Heap, M. J., Lavallée, Y., Laumann, A., Hess, K.-U., Meredith, P. G., and Dingwell, D. B.: How tough is tuff in the event of fire?, *Geology*, 40, 311–314, 2012.

Homand-Etienne, F. and Troalen, J.-P.: Behaviour of granites and limestones subjected to slow and homogenous temperature changes, *Eng. Geol.*, 20, 219–233, 1984.

20 Hurwitz, S., Christiansen, L. B., and Hsieh, P. A.: Hydrothermal fluid flow and deformation in large calderas: inferences from numerical simulations, *J. Geophys. Res.*, 112, B02206, doi:10.1029/2006JB004689, 2007.

Jones, C., Keaney, G., Meredith, P. G., and Murrell, S. A. F.: Acoustic emission and fluid permeability measurements on thermally cracked rocks, *Phys. Chem. Earth*, 22, 13–17, 1997.

25 Keshavarz, M., Pellet, F. L., and Loret, B.: Damage and changes in mechanical properties of a Gabbro thermally loaded up to 1000 °C, *Pure Appl. Geophys.*, 167, 1511–1523, doi:10.1007/s00024-010-0130-0, 2010.

Kolzenburg, S., Heap, M. J., Lavallée, Y., Russell, J. K., Meredith, P. G., and Dingwell, D. B.: Strength and permeability recovery of tuffsite-bearing andesite, *Solid Earth*, 3, 191–198, doi:10.5194/se-3-191-2012, 2012.

30 Lanari, R., Berardino, P., Borgstrom, S., Del Gaudio, C., De Martino, P., Fornaro, G., Guarino, S., Ricciardi, G. P., Sansosti, E., and Lundgren, P.: The use of IFSAR and classical geodetic techniques for caldera unrest episodes: application to the Campi Flegrei uplift event of 2000, *J. Volcanol. Geoth. Res.*, 133, 247–260, 2004.

Permeability and elastic moduli of tuff

M. J. Heap et al.

Title Page

Abstract

Introduction

Conclusions

References

Tables

Figures

◀

▶

◀

▶

Back

Close

Full Screen / Esc

Printer-friendly Version

Interactive Discussion



- Lockner, D.: The role of acoustic emission in the study of rock fracture, *Int. J. Rock Mech. Min.*, 30, 883–889, 1993.
- Lundgren, P., Usai, S., Sansosti, E., Lanari, R., Tesauro, M., Fornaro, G., and Berardino, P.: Modeling surface deformation observed with synthetic aperture radar interferometry at Campi Flegrei caldera, *J. Geophys. Res.*, 106, 19355–19366, 2001.
- Manconi, A., Walter, T. R., and Amelung, F.: Effects of mechanical layering on volcano deformation, *Geophys. J. Int.*, 170, 952–958, 2007.
- Manconi, A., Walter, T. R., Manzo, M., Zeni, G., Tizzani, P., Sansosti, E., and Lanari, R.: On the effects of 3-D mechanical heterogeneities at Campi Flegrei caldera, southern Italy, *J. Geophys. Res.*, B08405, doi:10.1029/2009JB007099, 2010.
- Mogi, K.: Relations between the eruptions of various volcanoes and the deformations of the ground surfaces around them, *Bull. Earthq. Res. Inst., Univ. Tokyo*, 36, 99–134, 1958.
- Nara, Y., Meredith, P. G., Yoneda, T., and Kaneko, K.: Influence of macro-fractures and micro-fractures on permeability and elastic wave velocities in basalt at elevated pressure, *Tectonophysics*, 503, 52–59, 2011.
- Orsi, G., D’Antonio, M., De Vita, S., and Gallo, G.: The Neapolitan Yellow Tuff, a large-magnitude trachytic phreatoplinian eruption: eruptive dynamics, magma withdrawal and caldera collapse, *J. Volcanol. Geoth. Res.*, 53, 275–287, 1992.
- Orsi, G., De Vita, S., and di Vito, M.: The restless, resurgent Campi Flegrei nested caldera (Italy): constraints on its evolution and configuration, *J. Volcanol. Geoth. Res.*, 74, 179–214, 1996.
- Orsi, G., Civetta, L., Del Gaudio, C., De Vita, S., Di Vito, M., Isaia, R., Petrazzuoli, S. M., Ricciardi, G. P., and Ricco, C.: Short-term ground deformations and seismicity in the resurgent Campi Flegrei caldera (Italy): an example of active block-resurgence in a densely populated area, *J. Volcanol. Geoth. Res.*, 91, 415–451, 1999.
- Peluso, F. and Arienzo, I.: Experimental determination of permeability of Neapolitan Yellow Tuff, *J. Volcanol. Geoth. Res.*, 160, 125–136, 2007.
- Plattner, C., Amelung, F., Baker, S., Govers, R., and Poland, M.: The role of viscous magma mush spreading in volcanic flank motion at Kīlauea Volcano, Hawai‘i, *J. Geophys. Res.*, 118, 2474–2487, 2013.
- Rosi, M. and Sbrana, A.: Phlegraean Fields: Quaderni de “La Ricerca Scientifica”: Consiglio Nazionale delle Ricerche Monograph 114, 9 p., 175 p. 1987.

Permeability and elastic moduli of tuff

M. J. Heap et al.

Title Page

Abstract

Introduction

Conclusions

References

Tables

Figures

◀

▶

◀

▶

Back

Close

Full Screen / Esc

Printer-friendly Version

Interactive Discussion



- Rutter, E.: On the nomenclature of mode of failure transitions in rocks, *Tectonophysics*, 122, 381–387, 1986.
- Saccorotti, G., Petrosino, S., Bianco, F., Castelluccio, M., Galluzzo, D., La Rocca, M., Del Pezzo, E., Zaccarelli, L., and Cusano, P.: Seismicity associated with the 2004–2006 renewed ground uplift at Campi Flegrei Caldera, Italy, *Phys. Earth Planet. Inter.*, 165, 14–24, 2007.
- 5 Sammonds, P., Dabrowa, A., Cheung, C., Smith, R., Meredith, P. G., De Natale, G., and Kilburn, C.: Physical and mechanical properties of Campi Flegrei Caldera borehole samples, Abstract, IAVCEI conference “Understanding Volcanoes”, Iceland 2008.
- Simmons, G. and Brace, W. F.: Comparison of static and dynamic measurements of compressibility of rocks, *J. Geophys. Res.*, 70, 5649–5656, 1965.
- 10 Todesco, M., Rinaldi, A. P., Bonafede, M.: Modelling of unrest signals in heterogenous hydrothermal systems. *J. Geophys. Res.*, 115, B09213, doi:10.1029/2010JB007474, 2010.
- Trasatti, E., Casu, F., Giunchi, C., Pepe, S., Solaro, G., Tagliaventi, S., Bernardino, P., Manzo, M., Pepe, A., Ricciardi, G. P., Sansosti, E., Tizzani, P., Zeni, G., and Lanari, R.: The 2004–2006 uplift episode at Campi Flegrei caldera (Italy): constraints from SBAS-DInSAR ENVISAT data and Bayesian source inference, *Geophys. Res. Lett.*, 35, L07308, doi:10.1029/2007GL033091, 2008.
- 15 Troise, C., Castagnolo, D., Peluso, F., Gaeta, F. S., Mastrolorenzo, G., and De Natale, G.: A 2-D mechanical–thermalfluid–dynamical model for geothermal systems at calderas: an application to Campi Flegrei, *J. Volcanol. Geoth. Res.*, 109, 1–12, 2001.
- Vanorio, T., Prasad, M., Patella, D., and Nur, A.: Ultrasonic velocity measurements in volcanic rocks: correlation with microtexture, *Geophys. J. Int.*, 149, 22–36, 2002.
- Vanorio, T., Virieux, J., Capuano, P., and Russo, G.: Three-dimensional seismic tomography from *P* wave and *S* wave microearthquake travel times and rock physics characterisation of the Campi Flegrei Caldera, *J. Geophys. Res.*, 110, B03201, doi:10.1029/2004JB003102, 2005.
- 20 Vinciguerra, S., Meredith, P. G., and Hazzard, J.: Experimental and modeling study of fluid pressure-driven fractures in Darley Dale sandstone, *Geophys. Res. Lett.*, L09609, doi:10.1029/2004GL019638, 2004.
- 30 Vinciguerra, S., Trovato, C., Meredith, P. G., Benson, P. M., Troise, C., and De Natale, G.: Understanding the seismic velocity structure of Campi Flegrei caldera (Italy): from the laboratory to the field scale, *Pure Appl. Geophys.*, 163, 2205–2221, 2006.

- Vinciguerra, S., Del Gaudio, P., Mariucci, M. T., Marra, F., Meredith, P. G., Montone, P., Pierdominici, S., and Scarlato, P.: Physical properties of tuffs from a scientific borehole at Alban hills volcanic district (central Italy), *Tectonophysics*, 471, 161–169, 2009.
- 5 Wohletz, K., Civetta, L., and Orsi, G.: Thermal evolution of the Phlegraean magmatic system, *J. Volcanol. Geoth. Res.*, 91, 381–414, 1999.
- Wong, T.-F. and Baud, P.: The brittle transition in rocks: a review, *J. Struct. Geol.*, 44, 25–53, 2012.
- Zamora, M., Sartoris, G., and Chelini, W.: Laboratory measurements of ultrasonic wave velocities in rocks from the Campi Flegrei volcanic system and their relation to other field data, *J. Geophys. Res.*, 99, 13553–13561, 1994.
- 10 Zhu, W. and Wong, T.-F.: The transition from brittle faulting to cataclastic flow: permeability evolution, *J. Geophys. Res.*, 102, 3027–3041, 1997.
- Zhu, W., Baud, P., Vinciguerra, S., and Wong, T.-F.: Micromechanics of brittle faulting and cataclastic flow in Alban Hills tuff, *J. Geophys. Res.*, 116, B06209, doi:10.1029/2010JB008046, 2011.
- 15

Permeability and elastic moduli of tuff

M. J. Heap et al.

Title Page

Abstract

Introduction

Conclusions

References

Tables

Figures

◀

▶

◀

▶

Back

Close

Full Screen / Esc

Printer-friendly Version

Interactive Discussion



Permeability and elastic moduli of tuff

M. J. Heap et al.

[Title Page](#)
[Abstract](#)
[Introduction](#)
[Conclusions](#)
[References](#)
[Tables](#)
[Figures](#)
[Back](#)
[Close](#)
[Full Screen / Esc](#)
[Printer-friendly Version](#)
[Interactive Discussion](#)


Table 2. Water permeability of Neapolitan Yellow Tuff (NYT) as a function of effective pressure and thermal stressing temperature.

effective pressure [MPa]	“as-collected” permeability [m ²]	Neapolitan Yellow Tuff (NYT)				
		100 °C permeability [m ²]	200 °C permeability [m ²]	300 °C permeability [m ²]	500 °C permeability [m ²]	750 °C permeability [m ²]
5	1.2×10^{-15}	1.7×10^{-15}	1.9×10^{-15}	2.7×10^{-15}	4.1×10^{-15}	1.1×10^{-14}
10	8.5×10^{-16}	1.7×10^{-15}	2.0×10^{-15}	2.7×10^{-15}	3.6×10^{-15}	1.1×10^{-14}
15	6.3×10^{-16}	1.6×10^{-15}	1.6×10^{-15}	2.4×10^{-15}	2.5×10^{-15}	8.5×10^{-15}
20	4.9×10^{-16}	1.1×10^{-15}	8.2×10^{-16}	1.6×10^{-15}	1.5×10^{-15}	6.1×10^{-15}
25	2.5×10^{-16}	7.6×10^{-16}	4.5×10^{-16}	1.2×10^{-15}	8.0×10^{-16}	4.4×10^{-15}
30	1.7×10^{-16}	5.3×10^{-16}	2.5×10^{-16}	8.6×10^{-16}	4.8×10^{-16}	3.2×10^{-15}
35	8.0×10^{-17}	5.3×10^{-16}	1.4×10^{-16}	6.4×10^{-16}	3.0×10^{-16}	1.8×10^{-15}
40	4.7×10^{-17}	3.1×10^{-16}	9.6×10^{-17}	5.3×10^{-16}	2.7×10^{-16}	3.1×10^{-16}
45	3.5×10^{-17}	2.3×10^{-16}	6.0×10^{-17}	4.1×10^{-16}	1.5×10^{-16}	5.4×10^{-17}
50	2.4×10^{-17}	1.7×10^{-16}	4.0×10^{-17}	3.2×10^{-16}	1.0×10^{-16}	3.3×10^{-17}

Permeability and elastic moduli of tuff

M. J. Heap et al.

Table 3. Water permeability of grey Campanian Ignimbrite (WGI) as a function of effective pressure and thermal stressing temperature.

effective pressure [MPa]	“as-collected” permeability [m ²]	Grey Campanian Ignimbrite (WGI)					
		100 °C permeability [m ²]	200 °C permeability [m ²]	300 °C permeability [m ²]	500 °C permeability [m ²]	750 °C permeability [m ²]	1000 °C permeability [m ²]
5	1.0×10^{-13}	7.8×10^{-14}	1.1×10^{-13}	1.0×10^{-13}	1.0×10^{-13}	1.0×10^{-13}	9.9×10^{-14}
10	9.7×10^{-14}	7.8×10^{-14}	1.1×10^{-13}	1.0×10^{-13}	9.7×10^{-14}	1.0×10^{-13}	9.4×10^{-14}
15	8.9×10^{-14}	6.8×10^{-14}	9.2×10^{-14}	9.5×10^{-14}	7.8×10^{-14}	9.8×10^{-14}	8.2×10^{-14}
20	7.4×10^{-14}	3.8×10^{-14}	6.7×10^{-14}	8.4×10^{-14}	4.9×10^{-14}	8.4×10^{-14}	6.2×10^{-14}
25	5.3×10^{-14}	2.4×10^{-14}	2.4×10^{-14}	6.3×10^{-14}	2.7×10^{-14}	4.0×10^{-14}	4.4×10^{-14}
30	2.5×10^{-14}	1.5×10^{-14}	8.6×10^{-15}	4.8×10^{-14}	1.4×10^{-14}	2.0×10^{-14}	3.2×10^{-14}
35	1.3×10^{-14}	1.2×10^{-14}	5.7×10^{-15}	3.7×10^{-14}	8.0×10^{-15}	1.2×10^{-14}	2.4×10^{-14}
40	7.9×10^{-15}	8.6×10^{-15}	4.6×10^{-15}	2.4×10^{-14}	5.5×10^{-15}	8.7×10^{-15}	1.9×10^{-14}
45	4.5×10^{-15}	6.0×10^{-15}	4.0×10^{-15}	1.9×10^{-14}	4.0×10^{-15}	6.6×10^{-15}	1.4×10^{-14}
50	2.2×10^{-15}	4.2×10^{-15}	3.5×10^{-15}	1.3×10^{-14}	3.0×10^{-15}	5.5×10^{-15}	1.1×10^{-14}

Title Page

Abstract

Introduction

Conclusions

References

Tables

Figures

◀

▶

◀

▶

Back

Close

Full Screen / Esc

Printer-friendly Version

Interactive Discussion



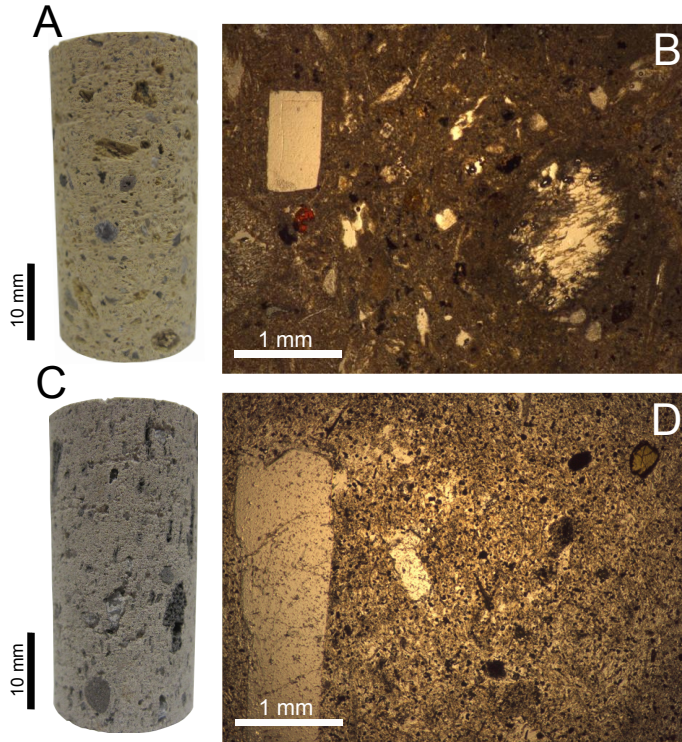


Fig. 1. Photographs and optical microscopy images of the as-collected Neapolitan Yellow Tuff (**A, B**) and Grey Campanian Ignimbrite (**C, D**). The photomicrographs are taken from Heap et al. (2012).

Permeability and elastic moduli of tuff

M. J. Heap et al.

Title Page

Abstract Introduction

Conclusions References

Tables Figures

◀ ▶

◀ ▶

Back Close

Full Screen / Esc

Printer-friendly Version

Interactive Discussion



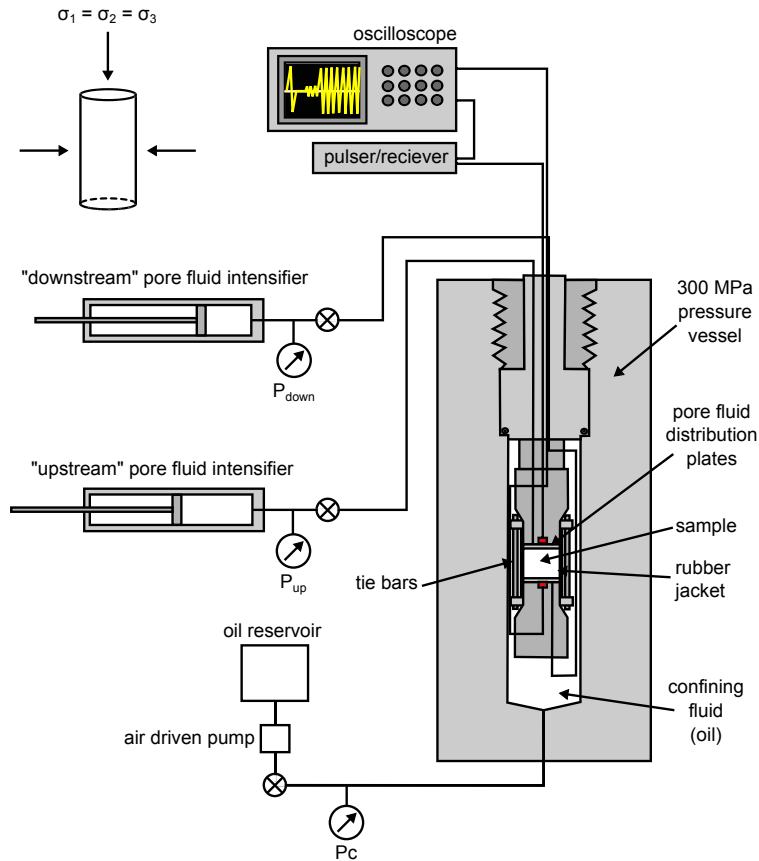


Fig. 2. Schematic diagram of the permeameter at the Rock & Ice Physics Laboratory (RIPL), University College London. Schematic is not to scale.

Title Page

Abstract

Introduction

Conclusions

References

Tables

Figures

◀

▶

◀

▶

Back

Close

Full Screen / Esc

Printer-friendly Version

Interactive Discussion



Permeability and elastic moduli of tuff

M. J. Heap et al.

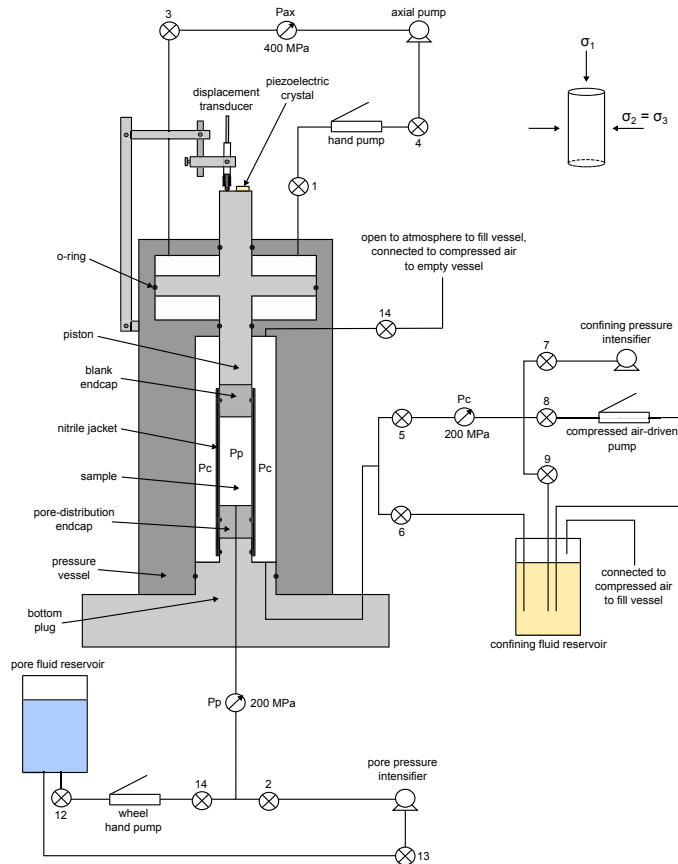


Fig. 3. Schematic diagram of the triaxial deformation apparatus at the Laboratoire de Déformation des Roches, Université de Strasbourg. Schematic is not to scale.

Title Page

Abstract Introduction

Conclusions References

Tables Figures

◀ ▶

◀ ▶

Back Close

Full Screen / Esc

Printer-friendly Version

Interactive Discussion

Permeability and elastic moduli of tuff

M. J. Heap et al.

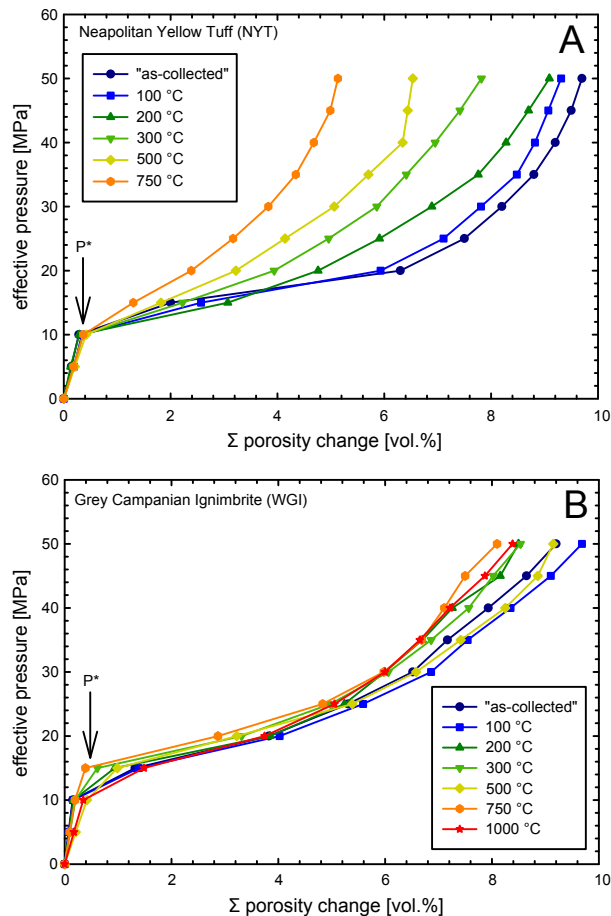


Fig. 4. The evolution of porosity change with increasing effective pressure for Neapolitan Yellow Tuff **(A)** and Grey Campanian Ignimbrite **(B)**. The temperatures in the legend refer to the thermal stressing temperature (see text for details).

Permeability and elastic moduli of tuff

M. J. Heap et al.

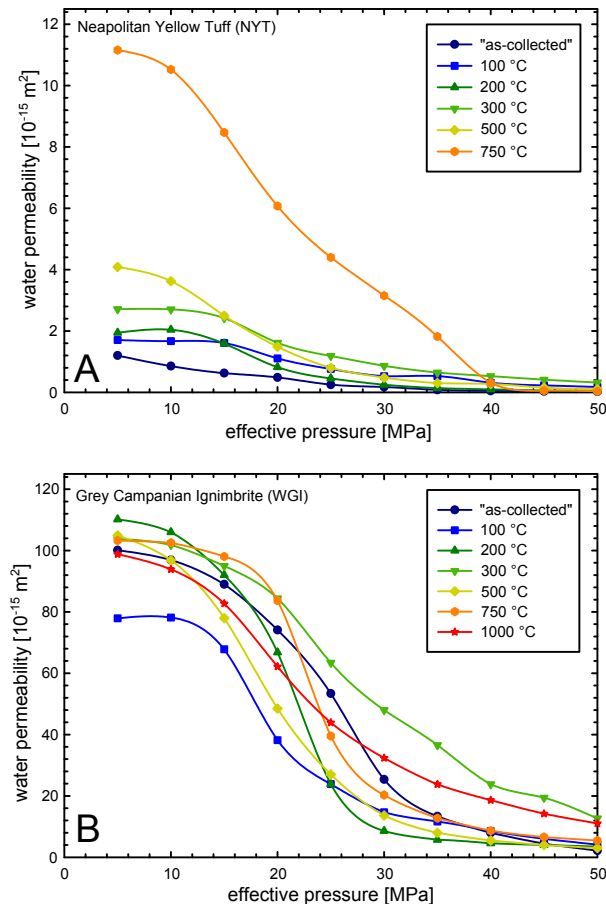


Fig. 5. The evolution of water permeability with increasing effective pressure for Neapolitan Yellow Tuff (A) and Grey Campanian Ignimbrite (B). The temperatures in the legend refer to the thermal stressing temperature (see text for details).

Permeability and elastic moduli of tuff

M. J. Heap et al.

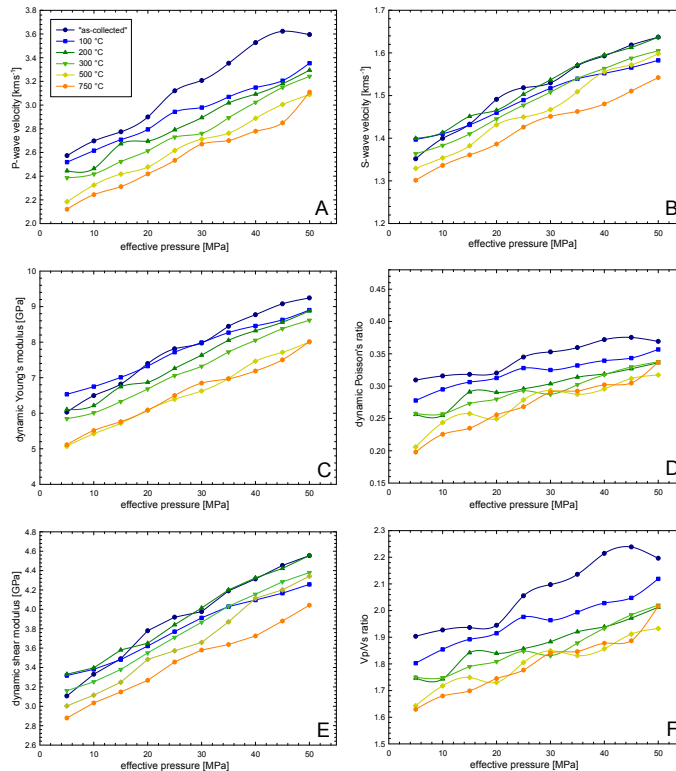


Fig. 6. The evolution of P wave velocity (**A**), S wave velocity (**B**), dynamic Young's modulus (**C**), dynamic Poisson's ratio (**D**), dynamic shear modulus (**E**), and V_P/V_S ratio (**F**) with increasing effective pressure for Neapolitan Yellow Tuff. The temperatures in the legend refer to the thermal stressing temperature (see text for details).

Permeability and elastic moduli of tuff

M. J. Heap et al.

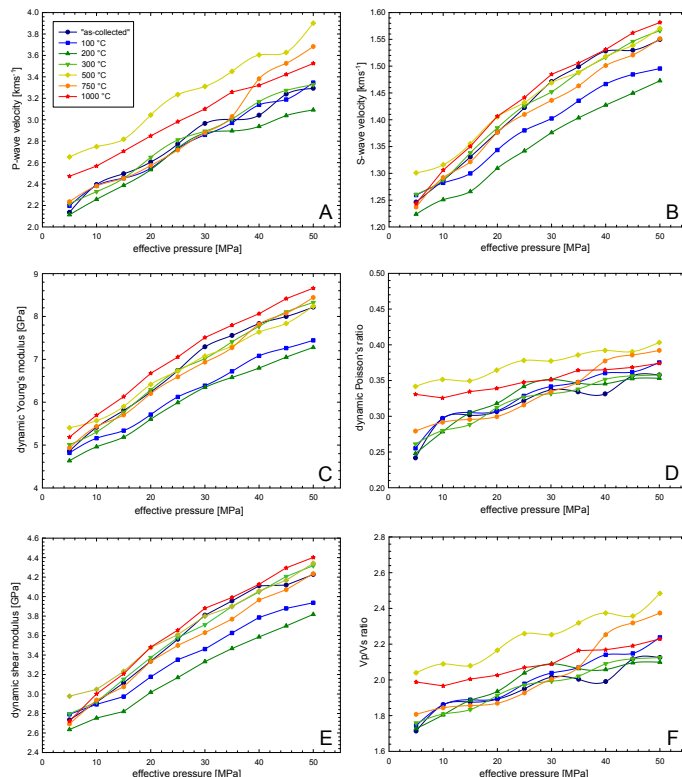


Fig. 7. The evolution of P wave velocity (**A**), S wave velocity (**B**), dynamic Young's modulus (**C**), dynamic Poisson's ratio (**D**), dynamic shear modulus (**E**), and V_P/V_S ratio (**F**) with increasing effective pressure for Grey Campanian Ignimbrite. The temperatures in the legend refer to the thermal stressing temperature (see text for details).

Permeability and elastic moduli of tuff

M. J. Heap et al.

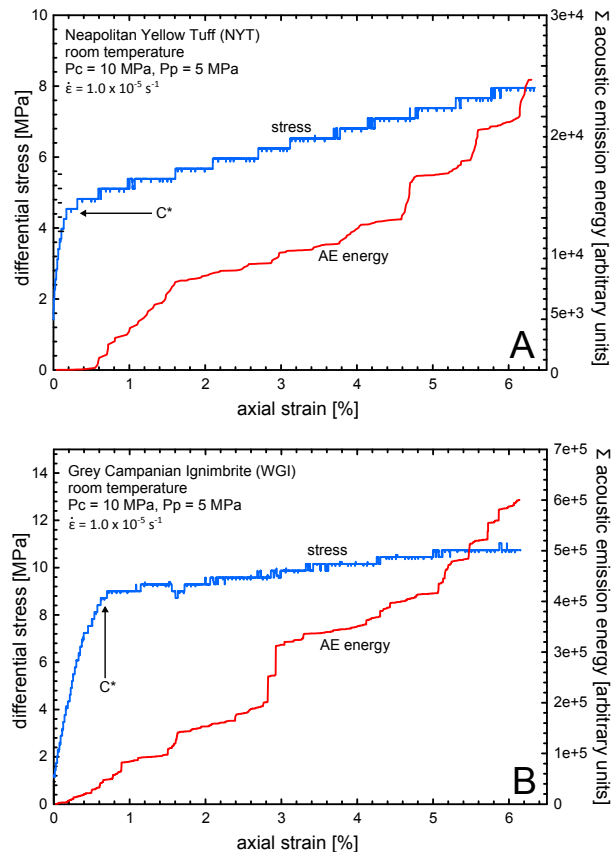


Fig. 8. Constant strain rate stress-strain curves, together with the cumulative output of acoustic emission (AE) “energy” (the area under the received AE waveform envelope) for as-collected Neapolitan Yellow Tuff **(A)** and Grey Campanian Ignimbrite **(B)**. The experimental conditions are provided on each panel and the positions of C^* are indicated by the arrows. The steps in the data are due to the stepwise nature of the pumps.

Permeability and elastic moduli of tuff

M. J. Heap et al.

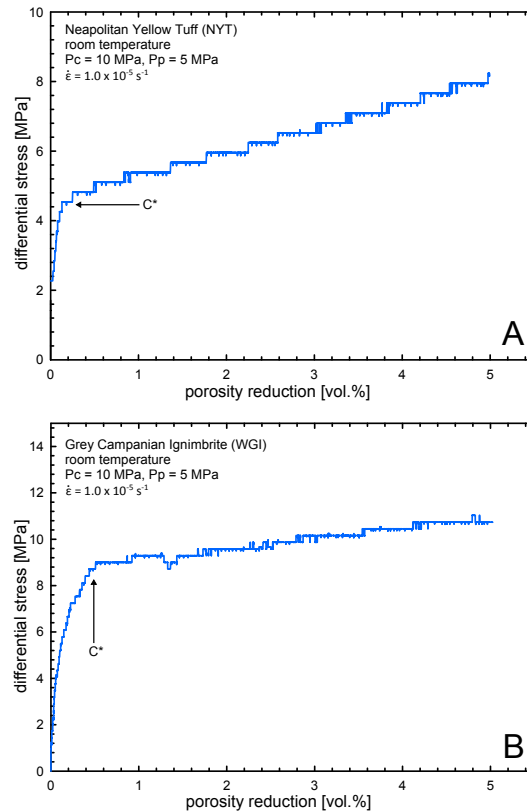


Fig. 9. Constant strain rate stress-porosity reduction curves for as-collected Neapolitan Yellow Tuff **(A)** and Grey Campanian Ignimbrite **(B)**. The experiments shown here are the same as those in Fig. 8. The experimental conditions are provided on each panel and the positions of C^* are indicated by the arrows. The steps in the data are due to the stepwise nature of the pumps.

Title Page

Abstract

Introduction

Conclusions

References

Tables

Figures

◀

▶

◀

▶

Back

Close

Full Screen / Esc

Printer-friendly Version

Interactive Discussion



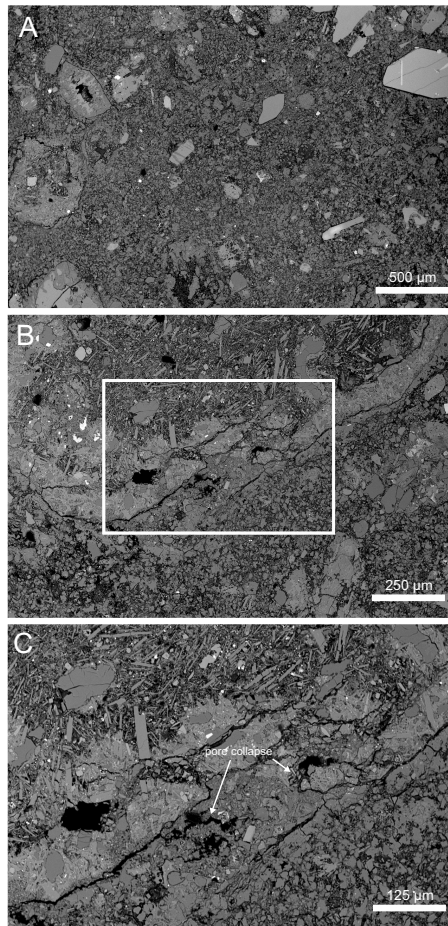


Fig. 10. Scanning electron microscope images of an as-collected sample of Neapolitan Yellow Tuff taken beyond P^* . **(B, C)** show evidence of pore collapse. **(C)** is a zoom of the white box shown in **(B)**.

Title Page

Abstract

Introduction

Conclusions

References

Tables

Figures

◀

▶

◀

▶

Back

Close

Full Screen / Esc

Printer-friendly Version

Interactive Discussion



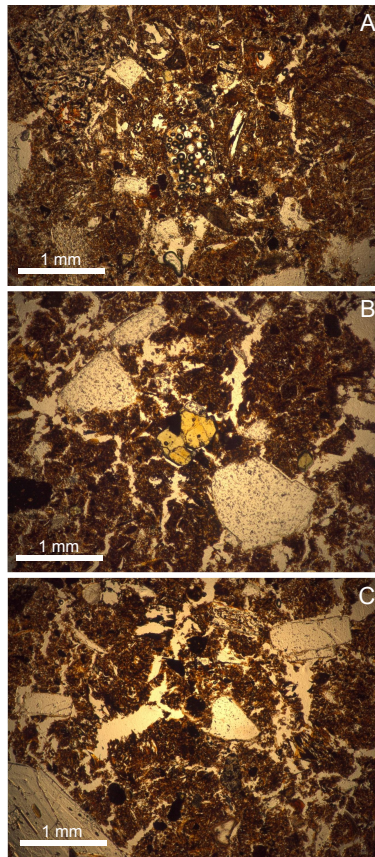


Fig. 11. Optical microscope images of Neapolitan Yellow Tuff thermally stressed to a temperature of 1000 °C showing macrocracks. The photomicrograph in **(A)**, showing foaming, is taken from Heap et al. (2012).

Permeability and elastic moduli of tuff

M. J. Heap et al.

Title Page

Abstract

Introduction

Conclusions

References

Tables

Figures

◀

▶

◀

▶

Back

Close

Full Screen / Esc

Printer-friendly Version

Interactive Discussion

